Aerosol lofting from sea breeze during INDOEX

S. Verma,[1] O. Boucher,[2] C. Venkataraman,[1] M. S. Reddy,[2,3] D. Müller,[4]
P. Chazette,[5] and B. Crouzille[2]

Abstract. This work was carried out to understand the mechanisms leading to lofting and large scale advection of aerosols over the Indian Ocean region due to interaction of sea breeze with the North East monsoon winds along the west coast of India. ECMWF wind fields for the months of February and March 1999 were analyzed at various times of day. Intense sea breeze activity was observed at 12 GMT (17:30 hrs local time) along the west coast of India with average intensity larger in March than in February. Sea breeze was seen to extend inland deeper in March than in February. Lofting of air observed as high as 800 hPa (approximately 2 km above sea level) could lead to entrainment of aerosols into the free troposphere and long range transport. Upward motion of air was observed everywhere along the west coast of India (from 8 to 20°N), on an average higher in March than in February, due to convergence between sea breeze and the synoptic-scale flow. A region of intense lofting of air and well-defined convergence was observed along the coast of the Karnataka region (12°N to 16°N). A simulation with a general circulation model nudged with ECMWF data indicated that the intrusion of marine air masses with low concentrations of organic matter (OM) is seen as deep as 64 km inland in the evening (15 GMT). Intrusion of sea-salt plume is seen to a maximum distance of around 200 km from 15 until 23 GMT. A well-developed lofted layer of aerosols as high as 3 km was also simulated during sea breeze activity along the west coast of India. The general circulation model simulation shows a clear diurnal evolution of the vertical profile of the aerosol extinction coefficient at Goa but fails to reproduce several features of the lidar observations, e.g. the marked diurnal variability of upper layers between 1 to 3 km. However, model simulates diurnal cycle at surface (0-0.7 km) which is not apparent in lidar measurements. The model simulates long range transport and captures the lofted plume downwind of the west coast of India. However, there is problem to simulate the timing and details of episodic lofted layers at Hulule, 700 km downwind of India.

1. Introduction

The intensive field phase of the Indian Ocean Experiment (INDOEX-IFP), was conducted during the northeast winter monsoon season, January-March 1999, to assess the role of aerosols on climate [*Ramanathan et al.*, 2001]. Extensive observational studies from multiple platforms established widespread anthropogenic aerosol loading over oceanic regions [*Lelieveld et al.*, 2001; *Krishnamoorthy et al.*, 2001; *Ball et al.*, 2003], . A striking feature was the presence, especially in March 1999, of multiple aerosol layers located above the boundary layer between 1 to 4 km in height. These elevated layers were observed at the continental stations of Goa and Dharwar on the west coast [*Leon et al.*, 2001;*Chazette*, 2003], over the ocean [*Reiner et al.*, 2001], and over in the Maldives, about a thousand kilometers downwind [*Müller et al.*, 2001a, 2001b; *Franke et al.*, 2003]. These layers contained anthropogenic aerosols including sulfate and other inorganic species, black carbon, organic carbon, and mineral dust [*Gabriel et al.*, 2002; *Mayol-Bracero et al.*, 2002; *Leon et al.*, 2001; *Chazette*, 2003]. In some occasion, they exhibited high extinction-to-backscatter ratios implying the presence of absorbing aerosols, potentially arising from biomass burning regions over India [*Franke et al.*, 2003]. According to *Raman et al.* [2002], the strength and coherence of the elevated plume was influenced by the diurnal variation of the structure of the upwind continental boundary layer.

Land and sea breeze are well known meteorological phenomena [*Miller et al.*, 2003]. Land- and sea-breeze systems are caused by the temperature differences over two surfaces. Sea breeze occurs at day when the land masses are hotter than the ocean, while land breeze occurs at night when land masses have cooled faster than the ocean. A detailed analysis of structure and impacts of sea breeze has recently been done by *Miller et al.* [2003]. It has been suggested that the aerosol lofting and large-scale advection during INDOEX was mediated by the interaction of the land- and sea-breeze cycle on the west coast of India with the regional-scale northeast monsoon flow, whereby aerosols can be lofted above the boundary layer and entrained into the regional-scale flow [*Leon et al.*, 2001]. The similar magnitude of aerosol optical depth (AOD) observed at Goa (coastal station, 73.13°E, 15.75°N) and Dharwar (150 km inland; 75.63°E, 15.7°N) suggested that aerosol loads are part of a large-scale feature. Also, the lack of temporal correlation in the surface concentrations of black carbon (BC) and the column AOD implied that the respective evolutions of aerosols in the boundary layer and the elevated layer were affected by distinct mechanisms, potentially emissions in the boundary layer and large

[1]Department of Chemical Engineering, Indian Institute of Technology Bombay, Mumbai, India
[2]Laboratoire d'Optique Atmosphérique, CNRS / Université des Sciences et Technologies de Lille, Villeneuve d'Ascq, France
[3]University Corporation for Air Research, NOAA-Geophysical Fluid Dynamics Laboratory, Princeton NJ
[4]Institute for Tropospheric Research, Leipzig, Germany
[5]Laboratoire des Sciences du Climat et de l'Environnment, CEA/CNRS, Gif-sur-Yvette, France

0148-0227/05/$9.00

scale transport in the elevated layer [*Leon et al.*, 2001]. The clear diurnal variability in the vertical extent and AOD of the elevated layer [*Chazette*, 2003] also suggested an effect of the sea breeze.

The first aerosol transport modeling studies of the INDOEX IFP have examined aerosol distributions, the contributions from different species to the AOD [*Collins et al.*, 2001; *Rasch et al.*, 2001], and a qualitative estimate of regional contributions to the aerosol load. Recently, *Minvielle et al.* [2004a, 2004b] modeled the transport of aerosols during INDOEX using a mesoscale model and explained the spatial and temporal distributions of aerosols (black carbon, sulfur dioxide, and soil dust) and their contribution to aerosol optical depth. Using a fine source classification and increased spatial resolution over the INDOEX domain in the general circulation model of the Laboratoire de Météorologie Dynamique (LMD-ZT), *Reddy et al.* [2004] demonstrated that sulfate and carbonaceous aerosols are main contributors to the AOD. They also showed that, although South Asian emissions contribute significantly to sulfate and carbonaceous aerosol loads over the Indian Ocean, large-scale transport from source regions outside South Asia was also important. This model study was extensively evaluated against INDOEX-IFP measurements and provides a useful tool to examine the mechanisms affecting large-scale advection of aerosols. These mechanisms have been previously examined using a meso-scale model for aerosol transport [*Leon et al.*, 2001]. However the model was run over a small domain (73°E to 76°E, 14°N to 16°N) and for a period of 48 hours only. Both *Leon et al.* [2001] and *Raman et al.* [2002] show a schematic representation of the interactions between the sea breeze and the large scale flow but do not present explicit model results showing the resulting aerosol distributions. The zoom facility of the LMD-ZT model gives us an opportunity to re-examine these issues using simulations on a larger domain and for a longer time period. Therefore, the specific objectives of the present study are (a) to simulate the aerosol transport during INDOEX-IFP in the LMD-ZT at an increased horizontal and vertical resolution, (b) evaluate the effects of sea breeze including the extent of inland incursion of winds and increase in vertical mass flux from convergence with the NE monsoon flow, (c) analyze the link between aerosol lofting from the sea-breeze circulation and large scale advection of elevated aerosol layers, as established in the observational studies, and (d) examine the model simulated diurnal variations of the elevated aerosol layers and their dependence on the sea-breeze circulation.

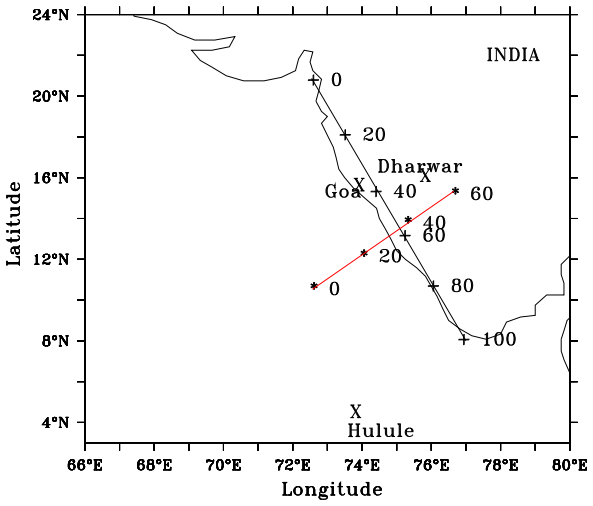

Figure 1. Region of focus and location of the coastal and transverse planes. The locations of Goa, Dharwar, and Hulule are indicated by crosses. Two consecutive marked points are at a distance of 275 and 160 km along the coastal and transverse planes, respectively. These points are referred with variable x in the text.

2. Method of study

2.1. ECMWF and observational data

The data set consists of horizontal (zonal and meridional) and vertical wind fields from meteorological analyze of the European Center for Medium Range Weather Forecast (ECMWF) for the months of February and March 1999. The data are provided on a regular latitude-longitude grid of 0.5°x0.5° over standard pressure levels (1000, 925, 850, 700, 500, 400, 300, 250, 200, 150, 100, 70, 50, 30, and 10 hPa). The dataset covers a window from 35°S-35°N and 30°E-110°E, with a temporal resolution of 6 hours (at 0, 6, 12, and 18 GMT).

The region of focus in the present study extends from 66°E to 80°E and 3°N to 24°N as shown in Figure 1. The analysis of the wind fields is carried out along different planes [Figure 1]. A coastal plane is located inland of the west coast and parallel to the coastline of India and runs from locations of Daman and Diu (0th point) to Thiruvanathapuram (100th point). The coastal plane is used to evaluate the vertical extent of air mass and aerosol lofting due to the convergence of the sea breeze with the regional-scale NE monsoon flow. A transverse plane is defined, which crosses the coastal plane, to analyze the vertical and horizontal extent of sea breeze circulation and lofting of air. These planes have been chosen within the zone of maximum convergence between sea breeze and North East monsoon winds.

The coastal stations of Goa and Dharwar are chosen to study the effects of sea breeze circulation. The station of Hulule located about 700 km off the coast is used to analyze the synoptic scale advection of aerosols over the ocean.

2.2. Short description of the LMD-ZT GCM

The study of lofting and synoptic-scale advection of aerosols is carried out with the help of the LMD-ZT general circulation model (GCM), version 3.3. A description of the model is given in *Boucher et al.* [2002] and *Reddy et al.* [2004]. Only a short description is repeated here.

In LMD-ZT atmospheric transport is computed with a finite volume transport scheme for large scale advection [*van Leer*, 1977; *Hourdin and Armangaud*, 1997], a scheme for turbulent mixing in the boundary layer, and a mass flux scheme for convection [*Tiedtke*, 1989]. The vertical transport of trace species is accounted for in updrafts, downdrafts, with entrainment and detrainment from and to the environment, and in the environment itself. The sulfur cycle has been incorporated and processes of convective transport, wet scavenging, and aqueous-phase chemistry have been parameterized as consistently as possible with the model physical parameterizations [*Boucher et al.*, 2002]. Sulfate formation, transport, and radiative forcing were estimated by *Boucher et al.* [2002]. The atmospheric cycles of carbonaceous aerosols, sea-salt, and dust are described in *Reddy and Boucher* [2004] and *Reddy et al.* [2004, 2005]. Emissions of SO_2, BC, and organic carbon (OC) from fossil fuel and biomass sources over Asia are from *Streets et al.* [2003], but emissions over India are from the high-resolution (0.25°x 0.25°) emission inventories of *Reddy and Venkataraman* [2002a, 2002b]. Aerosol optical properties (mass extinction coefficient– α_e, single scattering albedo– ω, and asymmetry factor– g) for all aerosol species are computed using Mie theory as described in *Reddy et al.* [2004]. The aerosol extinction coefficient is computed from all aerosol species and associated water.

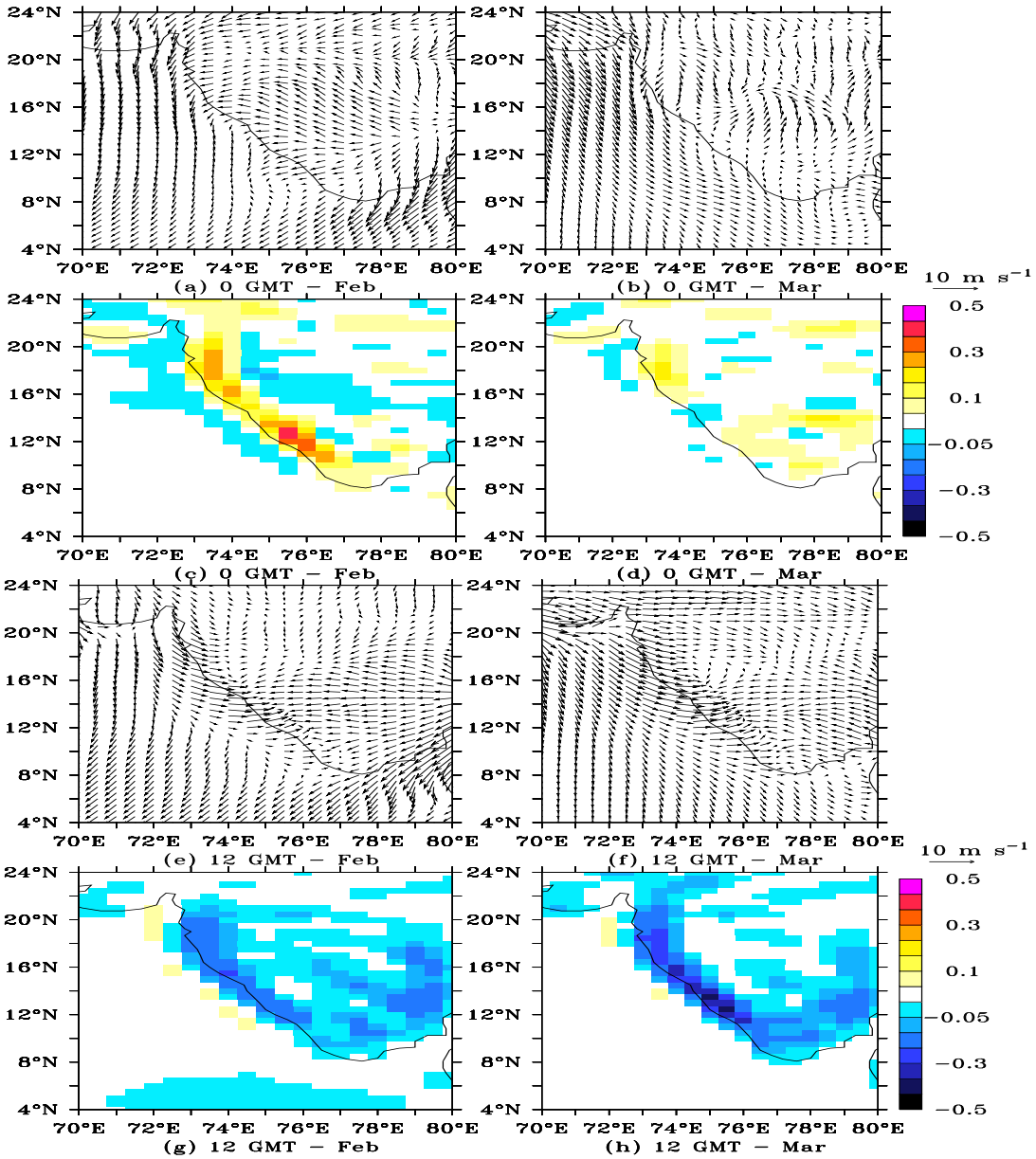

Figure 2. Vector of horizontal wind fields (ms^{-1}) at 1000 hPa and 0 GMT for (a) February, (b) March and at 12 GMT for (e) February and (f) March. Vertical wind velocity (Pa s^{-1}) at 1000 hPa and 0 GMT for (c) February, (d) March and at 12 GMT for (g) February and (h) March, 1999. Scale for wind velocity is indicated on right hand side of vector plots by an arrow representing 10 m s^{-1}.

3. Analysis of sea breeze using ECMWF analyzed wind fields

The ECMWF data were analyzed at various times of day (0, 6, 12, and 18 GMT) to identify the periods of sea-breeze activity. In February 1999 the sea breeze is observed at 12 GMT, corresponding to a local time of 17:30, but is absent at the other times of the day. In March 1999, sea breeze lasts longer from 6 to 18 GMT, with the largest intensity at 12 GMT. We therefore analyze the sea breeze related effects at 12 GMT for both months. The monthly mean surface horizontal wind fields for February and March 1999 at 0 and 12 GMT are shown in Figure 2. Convergence between the sea breeze and the synoptic-scale flow is observed everywhere along the west coast of India (from 8 to 20°N) at 12 GMT. The average horizontal surface wind speed at 12 GMT through the coastal plane (in the direction of the transverse plane) is 1.4 ms^{-1} in February. Significantly large values of 3.4 ms^{-1} were found for March. The larger intensity of the sea breeze in March is expected due to the higher temperature of Indian subcontinent in March [*Miller et al.*, 2003] that causes a larger contrast in temperature between ocean and land in March. The vertical wind velocity at 1000 hPa is also shown in Figure 2. Large negative values are observed at 12 GMT along the west coast, indicating convergence of air and subsequent upward motion. In contrast downward motion is observed at 0 GMT along the same coastal region. However this feature is only observed in February. The longer temporal extension of the sea breeze in March, from 6 to 18 GMT, is also evidenced in the maps of vertical velocities (not shown). The average velocity of upward motion at the surface along the coastal plane at 12 GMT is 0.24 Pa s^{-1} during March as compared to 0.12 Pa s^{-1} for February. Larger updrafts as observed in March from an analysis of ECMWF wind fields will have a greater potential for lofting of aerosols.

Fig. 3 represents the vertical profile of the vertical mass flux along the coastal plane. It shows upward rising of air as high as 800 hPa (approximately 2 km above sea level (asl)) all along the coastal plane with the largest intensity within points 40 to 70 (corresponding to the coordinates of 74.30°E, 15.80°N and 75.65°E, 11.90°N) along the west coast of India. The vertical profile of the vertical mass flux is also plotted along the transverse plane which has been chosen to lie within the region of intense upward motion defined above [Fig. 4]. We observe intense upward motion within points 35 to 45 (corresponding to the coordinates of 74.92°E, 13.30°N and 75.61°E, 14.12°N). It is interesting to note that the strongest upward motion does not occur at the surface but at higher altitudes. In March, the upward motion extends well above 800 hPa and as high as 600 hPa.

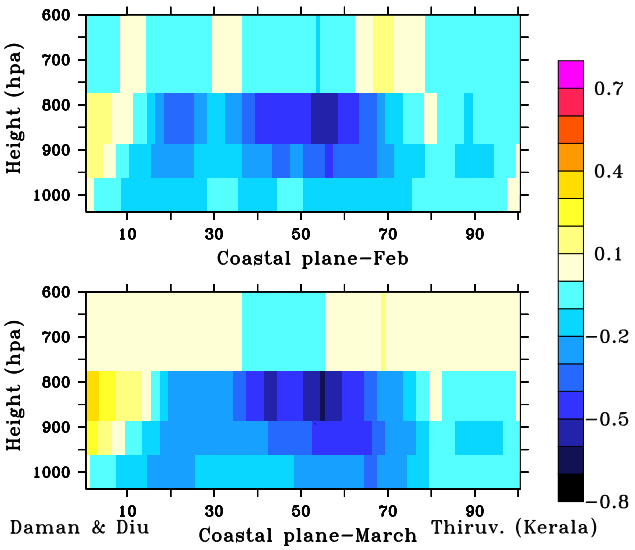

Figure 3. Monthly mean vertical mass flux of air (Pa s^{-1}) along the coastal plane at 12 GMT for (a) February and (b) March 1999.

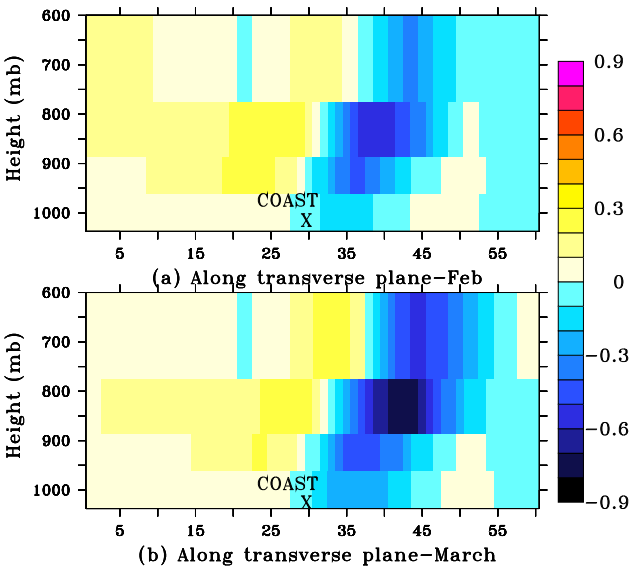

Figure 4. Monthly mean vertical mass flux of air (Pa s^{-1}) along the transverse plane at 12 GMT for (a) February and (b) March 1999.

The region of upward motion at 12 GMT is mostly located over land and is accompanied by a weaker downward motion off the coast. Figure 5 further shows the wind vectors in the transverse plane at 0 and 12 GMT for February and March. Sea breeze is seen to extend to about 100 km inland in February, but goes deeper to about 150 km inland in March.

In conclusion an area of well-defined convergence was found to occur around 12 GMT along the coastal plane with a maximum located at the coast of the Karnataka region. This location of well-defined convergence zone also justifies the optimum location of the coastal and transverse planes chosen for this study.

The mean altitude of the daily planetary boundary layer at the coastal location of Goa (73.08°E, 15.45°N) was observed to be close to 0.7 km throughout the complete measurement period [*Leon et al.*, 2001]. Lofting of air above 800 hPa (2 km asl) along the coast into and above the mixing zone of sea breeze circulation (1 km ASL) into the free troposphere due to convergence between sea breeze and the prevailing NE monsoon winds could lead to entrainment of aerosols into the free troposphere causing their large scale advection. Several observational studies over the Indian Ocean showed the presence of lofted aerosol layers during March 1999 (Table 1). The main reason for the observed layering over an island (4.1°N, 73.3°E) was believed to be the lofting of the continental air above the marine boundary layer when the pollution plumes are advected across the coastline [*Ansmann et al.*, 2000; *Franke et al.*, 2003].

4. Experimental setup of the LMD-ZT GCM

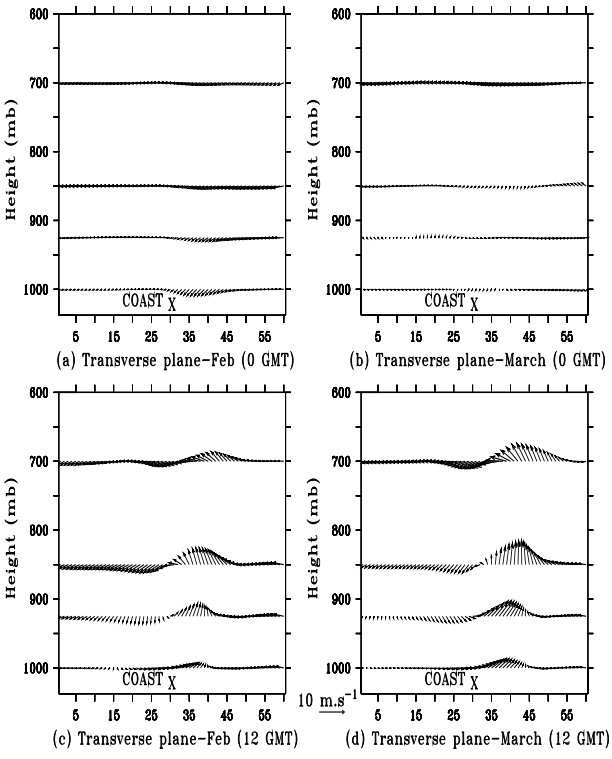

Figure 5. Vectors of the monthly mean horizontal wind in the transverse plane (ms^{-1}) and vertical wind velocity (x10 in Pa s^{-1}) for (a, c) February and (b, d) March 1999 at 0 and 12 GMT, respectively. The scale for the horizontal wind velocity is indicated between the two lower plots by an arrow representing 10 m s^{-1}

Table 1. Summary of observational studies showing the temporal and spatial extent of elevated aerosol plumes in 1999.

Period Pollution episodes	Platform	Region of study			Depth of elevated plume	Reference
		Station	Latitude	Longitude		
Feb. 18-Mar. 25	Lidar	Hulule	4.1°N	73.3°E	1000–3200 m	*Ansmann et al.* [2000], *Müller et al.* [2001a] *Pelon et al.* [2002], *Franke et al.* [2003] *Wagner et al.* [2001]
Feb.-Mar.	C-130 aircraft	-	8–15°N	70–85°E	1000–3200 m	*Reiner et al.* [2001], *Mayol-Bracero et al.* [2002], *Gabriel et al.* [2002]

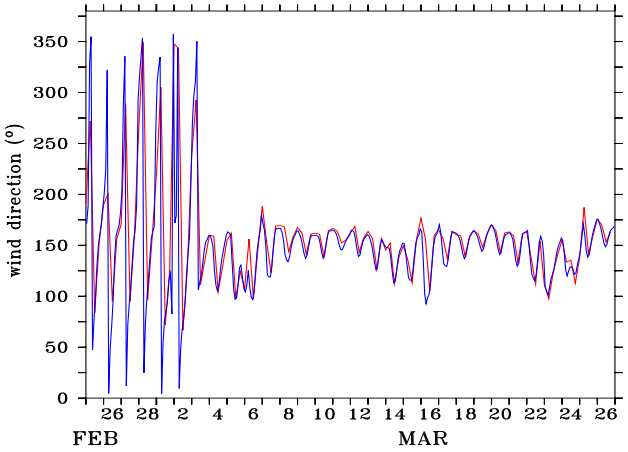

Figure 6. Temporal evolution of the wind direction from the GCM simulations (blue) and the original ECMWF analyze (red) for the period from February 25 to March 26 1999.

For this study the model resolution is increased from 96x72 to 192x145 points in longitude and latitude, respectively. The number of vertical layers has been increased to 50, with eleven layers below 850 hPa and eight layers between 850 and 500 hPa. A zoom is applied over the Indian region; it is centered at 75°E and 15°N and extends from 50°E to 100°E in longitude and from 5°S to 35°N in latitude. Zoom factors of 4 and 3 are applied in longitude and latitude, respectively, resulting in a resolution of about 0.47°x0.47° over the zoomed region. ECMWF global winds (at a resolution of 1.25°x1.25°) are re-gridded to the model grid. ECMWF INDOEX winds (at a resolution of 0.5°x0.5°, as described above), are also re-gridded to the model grid and pasted into the global wind dataset. These data are then used to nudge the model, with a relaxation time of 0.05 days. This ensures that the patterns of sea breeze, which are evident in the ECMWF data, are well captured by the model. Fig. 6 shows the direction of the surface wind at Goa from ECMWF analyze and from the model after nudging. It indicates that the model with nudging captures well the patterns of sea and land breeze from analyzed ECMWF winds.

We simulate the period from February 15 to March 26. Considering a 10 day spin up, we only examine model outputs from February 25 to March 26, with a time resolution of 2 hours for concentrations of sulfate, BC, organic matter (OM), and sea salt, and 30 minutes for the vertical profile of the extinction coefficient at Goa and Hulule.

5. Sea breeze effects on lofting and vertical distribution of aerosols

Movie caption: (om-3D.mpg and ss-3D.mpg) time evolution of the isosurface of OM or submicronic dry sea-salt concentration of 2 and 0.1 μg m^{-3} along the west coast of India during 20–26 March 1999. (om-2D.mpg and ss-2D.mpg) time evolution of the concentrations of OM and submicronic dry sea-salt in the transverse plane during 20–26 March 1999. The time resolution of all movies is 2 hours. The date and GMT time are indicated in the upper left corner.

This study is carried out with the help of a high-resolution simulation as described in section 4. We provide movies showing two- and three-dimensional representations of aerosol plumes as additional material. We concentrate on two species with similar lifetime but different origins, namely OM and submicronic sea salt. BC would show similar patterns as OM, while sulfate has both continental and maritime sources and would be more difficult to interpret.

Four different movies can be downloaded which show the evolution of OM and sea salt concentrations along the west coast of India (om-3D.mpg and ss-3D.mpg) and in the transverse plane (om-2D.mpg and ss-2D.mpg). Visualization of the 3D movies, time step by time step, reveals the effect of land and sea breeze on the aerosol plumes. On almost every day the isosurface of OM concentrations oscillates at the surface along the west coast of India. The isosurface of OM concentrations can also be seen to move up along the west coast at time around 21 GMT and later although not every day (it is particularly visible on March 20, 23, and 26). Another interesting feature in this movie (om-3D.mpg) is the transport of two elevated plumes coming from Africa, a first one on March 23-25 and a second one at higher altitude on March 25-26, which recirculate over the Northern Indian Ocean.

Visualization of the second movie (ss-3D.mpg) shows the movement of a sea-salt plume over the ocean and its episodic transport over the Indian continent. The plume of sea-salt is seen all along the coast from March 20 to March 22 and then shifts to somewhat higher latitude for the rest of March (approximately from x=0 to 70). It is worth noting a plume of sea-salt on March 24 entering deep inside the continent and then being lofted to higher altitudes. Lofting occurs every day between March 24 and 26 and reaches its maximum intensity around 13 or 15 GMT.

A further detailed visualization of transport of these species during periods of land and sea breeze activity is made with the help of 2D movies (see Fig. 1) for the same period of time (movies om-2D.mpg and ss-2D.mpg). These movies represent the vertical distribution of OM and dry sea-salt concentrations in the transverse plane.

The om-2D.mpg movie confirms the timing of the features discussed above. The sea breeze affects the concentration at the surface most at 13-17 GMT while the lofting occurs later at 21 GMT. It is also clear that the lofting occurs quite inland (points x=45 to 60) and rarely along the coast (x=30). Marine air masses with low concentrations of OM appears move inland (till x=38 points) to a maximum distance of around 64 km from the coast at around 15 GMT. The plume then travels off the coast (1 to 7 GMT) and hence represents the effect of land and air masses on concentration of OM.

Visualization of movie on the same plane for sea-salt (ss-2D.mpg) for the same period shows a plume of sea-salt during the first 2 days (20-22 March) followed by a calm period with low sea-salt concentrations. The sea-salt plume moves inland (till x=55 points) to a maximum distance of around 200 km on 20 and 21 March from 15 until 23 GMT, which seems to last longer than for OM. We see lofting of sea-salt at x values of 35 to 45 points on 20 March and 30 to 45 points on 21 March. Lofting occurs closer to the coast at 13-17 GMT, which is a bit earlier than for OM.

A further analysis of the effects of sea breeze on the vertical distribution and lofting of aerosols is performed by looking at their vertical profiles along the transverse and coastal planes (depicted on Fig. 1). The distributions are examined at 11 and 23 GMT, which are the times of maximum contrast. Fig. 7 represents the vertical profile of OM and sea-salt in the transverse plane as an average for the period from 21-25 March at 11 and 23 GMT. The isocontours for OM concentrations above land are slanted towards the continent at 11 GMT but are vertical at 23 GMT, which indicates stronger vertical mixing at that time. The export of OM to the ocean is also larger at that time while at 11 GMT the plume over the ocean exhibits a maximum at x=25 and is decoupled from that inland. Consistently the sea-salt plume extends higher up at 23 GMT as compared to 11 GMT.

Fig. 8 presents the OM concentrations along the coastal plane. The formation of a plume decoupled from the surface is evident at 23 GMT between x equal to 30 to 80 along the west coast. This corresponds to the region of maximum vertical mass flux of air according to Fig. 3. A similar analysis made on planes parallel to the coastal plane (within longitudes 66 to 75°E and north to 5°N) shows the lofted plume to be a permanent feature within x=20 to 70 points (i.e., between 10 and 18°N) and an episodic feature south to 10°N. This corroborates the C-130 observations of high concentration of sulfate and aerosol species around 10°N [*Gabriel et al.*, 2002; see Table 1].

6. Local- and meso-scale effects of the sea-breeze circulation on long-range transport

These studies are carried out at the coastal station of Goa (15.45°N, 73.08°E) to evaluate the local effects of sea breeze circulation. This study is further extended to understand the presence of lofted aerosol layers at Hulule (4.4°N, 73.5°E; 700 km downwind to Indian coast) and the impact of sea breeze on the long range transport.

Fig. 9 shows the temporal evolution of the aerosol extinction coefficient at Goa during March 1-15th, 1999 with estimates from the LMD-ZT GCM and from the lidar measurements [*Chazette*, 2003]. Fig. 9a reveals the presence of diurnal variations in the extinction coefficient close to

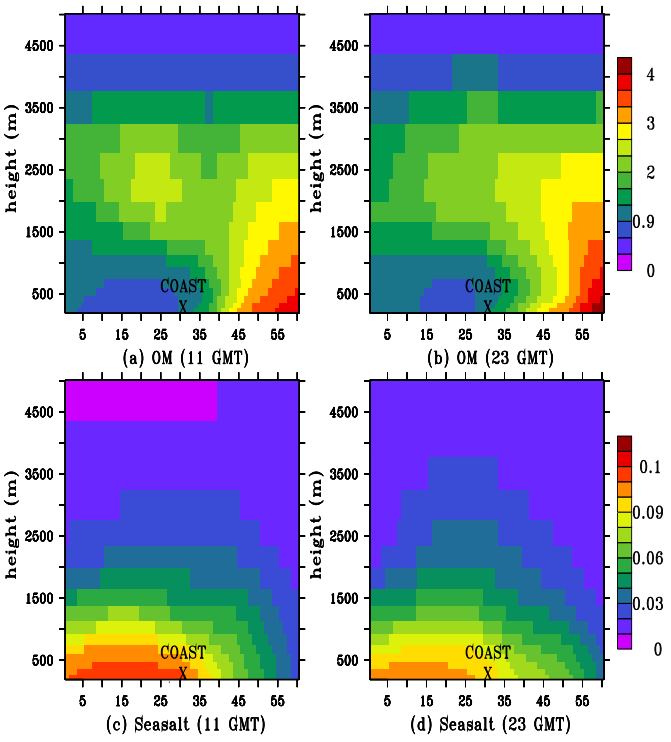

Figure 7. Vertical distribution of the average aerosol concentrations (μg m^{-3}) along the transverse plane for (a) OM, (b) sea-salt at 11 GMT and (c) OM, and (d) sea-salt at 23 GMT for the period 21–25 March 1999.

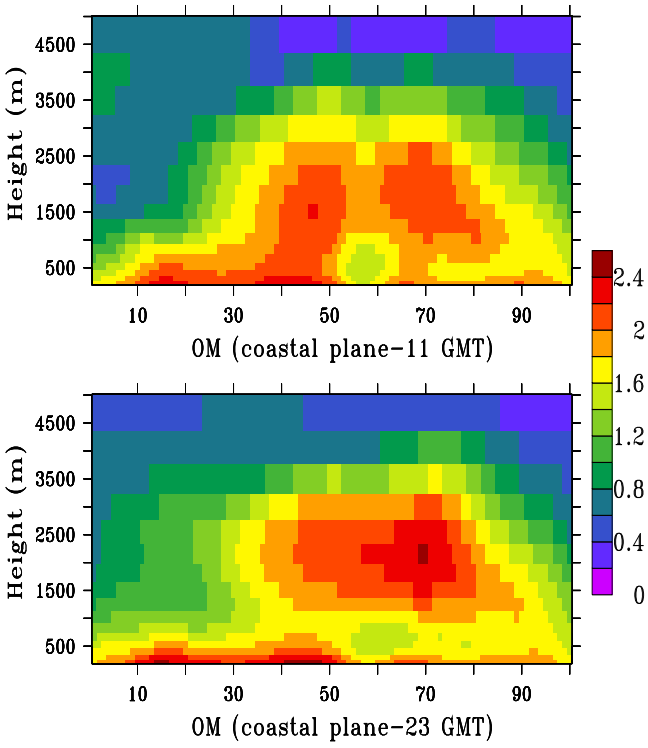

Figure 8. Vertical distribution of average aerosol concentrations (μg m^{-3}) along the coastal plane for OM at 11 and 23 GMT for the period from 21-25 March 1999.

the surface (0-0.7 km). The maximum extinction coefficient occurs around 12 GMT at the surface and propagates upwards. At 1 km altitude, the maximum occurs around 0 GMT. The GCM also captures some diurnal variations at higher altitude (1.5-3 km) but it is masked by day-to-day variability. For the period 5 to 8 March, the average extinction coefficient at 1.5-3 km peaks at 18 GMT. The temporal evolution of the aerosol extinction coefficient from the lidar measurements is shown in Fig. 9b. The surface aerosol layer is well mixed over the altitude range of 0.11 to 0.7 km and does not show a clear diurnal variability. However, the layer between 0.7 and 4 km shows larger extinction coefficient during nighttime than daytime [*Chazette*, 2003]. There are both areas of agreement and disagreement between the modeled and observed aerosol profiles at Goa. The model simulates a diurnal cycle at the surface which is not really seen in the lidar profiles, but which is in agreement with surface-based measurements of the scattering coefficient, with larger values during nighttime (Fig. 8 from *Chazette* [2003]). The variability in the upper layer (1.5-3 km) is less marked in the model than in the observations, but is in phase with observations for the period 6-8 March. The model underestimates the aerosol extinction coefficient in the surface layer but spreads the layer too much over the vertical, which tends to largely overestimate it in the 1 to 3.5 km altitude range. This provides an explanation as to why the model under predicts surface concentrations over India as mentioned by *Reddy et al.* [2004].

Fig. 10 shows the vertical profile of the aerosol extinction coefficient as derived from a six-wavelength lidar at Hulule [*Müller et al.*, 2001a, 2001b] and as estimated by the LMDZT GCM. Measurements are available for two periods (6–10 March) and (17–24 March) with profiles restricted to altitude larger than 1 km. The minimum height is given by the incomplete overlap between laser beam and the field-of-view of the receiver telescope. For a detailed explanation we refer to *Franke et al.* [2003]. Below 1 km height a mean extinction coefficient was derived on the basis of the particle backscatter coefficients, which reach almost down to the surface, and information on optical depth below 1 km height, which was derived from Raman lidar observations

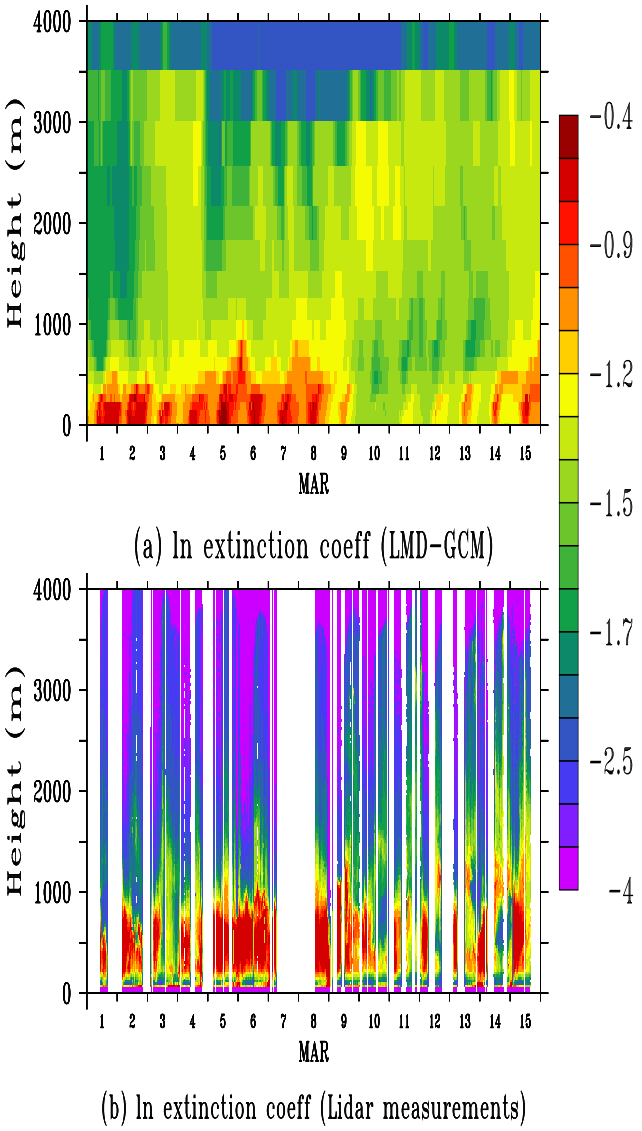

Figure 9. Temporal evolution between 1 and 15 March 1999 of the aerosol vertical profile (log to the base of 10 of the aerosol extinction coefficient in unit of km^{-1}) from (a) the GCM simulation and (b) the lidar measurements of *Chazette* [2003]. The x-axis corresponds to days in March for GMT time. The lidar measurements should not be trusted in the first 200 meters because of incomplete overlap between the lidar beam and the receiver field of view

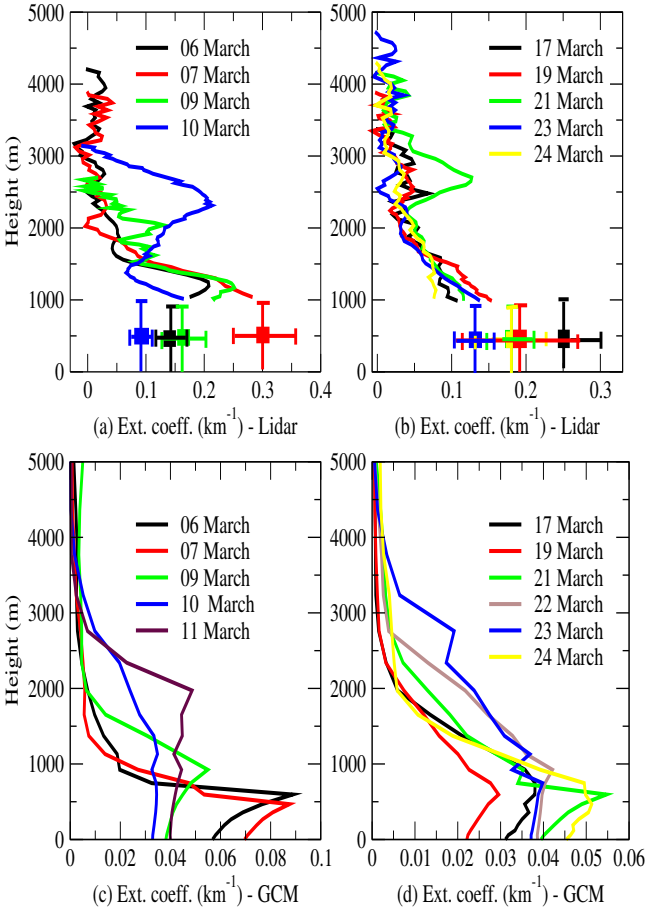

Figure 10. Vertical profile of the aerosol extinction coefficient (km^{-1}) from lidar measurements (top panels, [*Müller et al.*, 2001a, 2001b]) and the GCM simulation (bottom panels) at Hulule for the period from 6 to 11 March 1999 (left panels) and 17 to 24 March 1999 (right panels).

after sunset and sun photometer observations carried out at Hulule close to sunset [*Franke et al.*, 2003]. Each profile is the mean of approximately 2 hours of measurement. In general the aerosol extinction coefficient decreases with height except for 10 March and 21 March, where elevated plumes are seen at altitude ranges of 2 to 3 km. The model profiles, which have been averaged over the measurement times, do not show these elevated plumes. However it is encouraging to see that the extinction coefficient on 11 March peaks at 2 km altitude. The vertical profile of backscatter coefficient from lidar observations also shows similar features on March 11 at 2 km altitude (Figure not shown here). For the period from 17 to 24 March, the lofted layer of 21 March is not captured by the model (Fig. 10b). A small lofted feature seen in lidar measurements on 23 March at about 3 km also appears on the 23rd in the model between 2-3 km height [Fig. 10d]. We also show the time evolution of the vertical profile of the extinction coefficient at Hulule for the full period of simulation in Fig. 11. Fig. 11 shows the presence of lofted layers on March 11 and March 23 between 2-2.5 km height. It also shows episodes of lofted layers on March 9, and 24 at about 1-2 km height and on February 26, and March 5, 6, 20, and 21 at about 0.5-1 km. Lofted features seen in model on March 6 at 0.5-1 km is visible in lidar profiles at around 1 km height. Lofted feature seen in model on March 9 at 1-2 km height is visible in lidar profile at around 1.2 km height [Figure 10 (a)]. It appears that the model is not able to capture the episodic periods of lofted layers [March 10, 21]. It shows up the lofted features of lidar profiles on other days [March 6, 9, 21] but not at the exact period of averaging of measurements with the correct magnitude of observed extinction coefficient. The model underestimates the extinction coefficient by a factor of 5 to 6 as compared to measurements. We believe that this is due to both an overestimation of the precipitation rate over the Arabian Sea [*Reddy et al.*, 2004] and inaccuracies in the wind fields of ECMWF which are used to nudge the model [*Bonazzola et al.*, 2001] .

7. Conclusions

Analysis of wind field data from ECMWF showed the presence of intense sea breeze activity at 12 GMT (17:30 local time) along the west coast of India. The average intensity of sea breeze is (1.4 ms^{-1}) in February. Significantly larger values of 3.4 ms^{-1} were found for March. Upward mass flux of air was observed everywhere along the west coast of India (from 8 to 20°N) due to convergence between the sea breeze and the North East monsoon winds with higher intensity of upward motion observed in March (0.24 Pa s^{-1}) as compared to February (0.12 Pa s^{-1}) and hence greater potential for aerosol lofting. Lofting of air above 800 mb (2 km asl) along the coast leads to entrainment of aerosols into the free troposphere causing their large scale advection. To study the effects of sea breeze on aerosols, a general circulation model (GCM) was nudged with ECMWF wind fields to ensure that the model captures the patterns of sea breeze which are evident in the ECMWF data. The model simulates the concentrations of different aerosol species as well as the aerosol extinction coefficient, which were analyzed to study effects of sea breeze on the vertical distribution and lofting of aerosols. The model results are compared to observations at the coastal station of Goa and at Hulule, 700 km downwind, in order to understand the local and meso-scale effects of sea breeze circulation and long range transport. A well developed lofted layer of aerosols as high as 3 km is estimated for the period averaged from March 21 to March 25 along the west coast of India. This period corresponds to episodes of pollution layers observed over the Indian Ocean region. The model simulates diurnal variations due to local sea breeze effects in the aerosol extinction coefficient at Goa but fails to reproduce the marked diurnal variability of upper layers between 1 to 3 km as seen in lidar observations. The model simulates diurnal cycle at surface (0-0.7 km) which is not apparent in lidar measurements. The model also simulates long-range transport, 700 km downwind the west coast of India. However there is problem to simulate the timing and details of episodic lofted layers at Hulule. We believe that a thinner vertical resolution and better analyzed wind wields [*Bonazzola et al.*, 2001] are needed to improve the simulations of long-range transport of aerosol layers over this region.

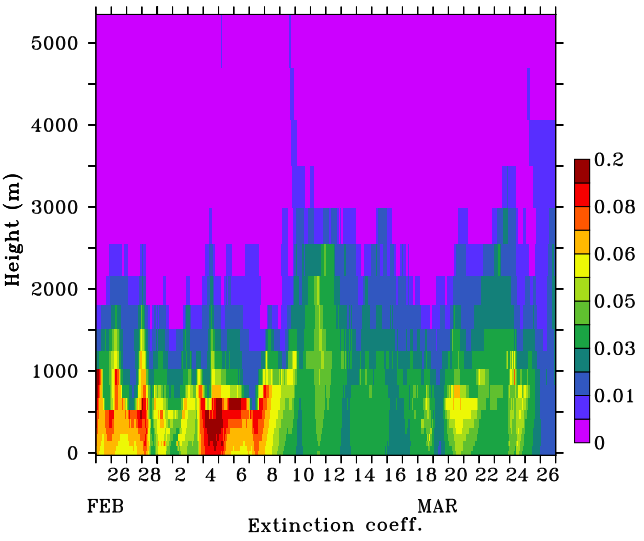

Figure 11. Simulated temporal evolution between 25 February and 26 March 1999 of the vertical profile of the aerosol extinction coefficient (km^{-1}) at Hulule.

Acknowledgments. This work was supported at Indian Institute of Technology Bombay through a grant from the Indian Ministry for Human Resource Development. We are thankful to the European Center for Medium Range Weather Forecast (ECMWF) and the Institut Pierre Simon Laplace (IPSL) for providing us with analyze of wind fields. A significant part of this work was accomplished through computing time provided by the "Institut du Développement et des Ressources en Informatique Scientifique" (IDRIS) of the CNRS under projects 031167 and 041167. S. Verma acknowledges support from START and the French Embassy in India for her two visits to LOA (France). This study is part of a collaborative project also supported by the Indo-French Center for the Promotion of Advanced Research (IFCPAR).

References

Ansmann, A., D. Althausen, U. Wandinger, K. Franke, D. Müller, F. Wagner, and J. Heintzenberg (2000), Vertical profiling of the Indian aerosol plume with six-wavelength lidar during INDOEX: A first case study, *Geophys. Res. Lett.*, *27(7)*, 963–966.

Ball, W., R. Dickerson, B. Doddridge, J. Stehr, T. Miller, D. Savoie, and T. Carsey (2003), Bulk and size aggregated aerosol composition observed during INDOEX 1999: Overview of meteorology and continental impacts, *J. Geophys. Res.*, *108*(D10), 8001, doi:10.1029/2002JD002467.

Bonazzola, M., L. Picon, H. Laurent, F. Hourdin, G. Sèze, H. Pawlowska, and R. Sadourny (2001), Retrieval of large-scale wind divergences from infrared Meteosat-5 brightness temperatures over the Indian Ocean, *J. Geophys. Res.*, *106*(D22), 28,113–28,128.

Boucher, O., M. Pham, and C. Venkataraman (2002), Simulation of the atmospheric sulphur cycle in the Laboratoire de Météorologie Dynamique general circulation model: Model description, model evaluation and global and European budgets, *Note Scientifique de l'Institut Pierre Simon Laplace n° 23, Paris, France.*

Chazette, P. (2003), The monsoon aerosol extinction properties at Goa during INDOEX as measured with lidar, *J. Geophys. Res.*, *108*(D10), 4187, doi:10.1029/2002JD002074.

Collins, W., P. Rasch, B. Eaton, B. Khattatov, J. Lamarque, and C. Zender (2001), Simulating aerosols using a chemical transport model with assimilation of satellite aerosol retrievals: Methodology for INDOEX, *J. Geophys. Res.*, *106(D7)*, 7313–7336.

Franke, K., A. Ansmann, D. Müller, D. Althausen, C. Venkataraman, M. S. Reddy, and R. Scheele (2003), Optical properties of the Indo-Asian haze layer over the Tropical Indian Ocean, *J. Geophys. Res.*, *108*(D2), 4069, doi:10.1029/2002JD002473.

Gabriel, R., O. Mayol-Bracero, and M. Andreae (2002), Chemical characterisation of submicron aerosol particles collected over the Indian Ocean, *J. Geophys. Res.*, *107*(D19), 8005, doi:10.1029/2000JD000034.

Hourdin, F., and A. Armangaud (1997), The use of finite-volume methods for atmospheric advection of trace species. Part 1: Test of various formulations in a general circulation model, *Mon. Weath. Rev.*, *127*, 822–837.

Krishnamoorthy, K., A. Saha, B. Prasad, K. Niranjan, D. Jhurry, and P. Pillai (2001), Aerosol optical depths over peninsular India and adjoining oceans during the INDOEX compaigns: Spatial, temporal, and spectral characteristics., *J. Geophys. Res.*, *106(D22)*, 28,539–28,554.

Lelieveld, J., et al. (2001), The Indian Ocean Experiment: Widespread air pollution from South and Southeast Asia, *Science*, *291*, 1031–1036.

Leon, J.-F., et al. (2001), Large scale advection of continental aerosols during INDOEX, *J. Geophys. Res.*, *106(D22)*, 28,427–28,440.

Mayol-Bracero, O., R. Gabriel, M. Andreae, T. Kirchstetter, T. Novakov, J. Ogren, P. Sheridan, and D. Streets (2002), Carbonaceous aerosols over the Indian Ocean during INDOEX: Chemical characterisation, optical properties and probable sources, *J. Geophys. Res.*, *107*(D19), 8030, doi:10.1029/2000JD000039.

Miller, S., B. Keim, R. Talbot, and H. Mao (2003), Sea breeze: Structure, forecasting, and impacts, *Rev. Geophys.*, *41*(3), 1011, doi:10.1029/2003RG000124.

Minvielle, F., et al. (2004a), Modeling of the transport of aerosols during INDOEX 1999 and comparison with experimental data, Part 1: Carbonaceous aerosol distribution, *Atmos. Env.*, *38(12)*, 1811–1822.

Minvielle, F., et al. (2004b), Modeling transport of aerosols during INDOEX 1999 and comparison with experimental data, Part 2: continental aerosol and their optical depth, *Atmos. Env.*, *38(12)*, 1823–1837.

Müller, D., K. Franke, F. Wagner, D. Althausen, A. Ansmann, and J. Heintzenberg (2001a), Vertical profiling of optical and physical particle properties over the tropical Indian Ocean with six-wavelength lidar 1. Seasonal cycle, *J. Geophys. Res.*, *106(D22)*, 28,567–28,575.

Müller, D., K. Franke, F. Wagner, D. Althausen, A. Ansmann, and J. Heintzenberg (2001b), Vertical profiling of optical and physical particle properties over the tropical Indian Ocean with six-wavelength lidar 2. Case studies, *J. Geophys. Res.*, *106(D22)*, 28,577–28,595.

Pelon, J., C. Flamant, P. Chazette, J.-F. Léon, D. Tanré, M. Sicard, and S. Satheesh (2002), Characterisation of aerosol spatial distribution and optical properties over the Indian Ocean from airborne lidar and radiometry during INDOEX 99, *J. Geophys. Res.*, *107*(D19), 8029, doi:10.1029/2001JD000402.

Raman, S., D. Niyogi, M. Simpson, and J. Pelon (2002), Dynamics of elevated plume over the Arabian Sea and the Northern Indian Ocean during northeasterly monsoons and during the Indian Ocean experiment (INDOEX), *Geophys. Res. Lett.*, *29*(16), doi:10.1029/2001GL014193.

Ramanathan, V., et al. (2001), An integrated analysis of the climate forcing and effects of the great Indo-Asian haze, *J. Geophys. Res.*, *106(D22)*, 28,371–28,398.

Rasch, P., W. Collins, and B. Eaton (2001), Understanding the Indian Ocean Experiment (INDOEX) aerosol distributions with an aerosol assimilation, *J. Geophys. Res.*, *106(D7)*, 7337–7355.

Reddy, M. S., and O. Boucher (2004), Global carbonaceous aerosol transport and assessment of radiative effects in the LMDZ GCM, *J. Geophys. Res.*, *109*(D14), D14202, doi:10.1029/2003JD004048.

Reddy, M. S., and C. Venkataraman (2002a), Inventory of aerosol and sulphur dioxide emissions from India: I - Fossil fuels combustion, *Atmos. Env*, *36*, 677–697.

Reddy, M. S., and C. Venkataraman (2002b), Inventory of aerosol and sulphur dioxide emissions from India: II - Biomass combustion, *Atmos. Env.*, *36*, 699–712.

Reddy, M. S., O. Boucher, C. Venkataraman, S. Verma, J.-F. Leon, and M. Pham (2004), GCM estimates of aerosol transport and radiative forcing during INDOEX, *J. Geophys. Res.*, *109*(D16), D16205, doi:10.1029/2004JD004557.

Reddy, M. S., O. Boucher, N. Bellouin, M. Schulz, Y. Balkanski, and M. Pham (2005), Estimates of multi-component aerosol optical depths and direct radiative perturbation in the LMDZT general circulation model, *J. Geophys. Res.*, *in press*, doi:10.1029/2004JD004757.

Reiner, T., D. Sprung, C. Jost, R. Gabriel, O. Mayol-Bracero, M. Andreae, T. Campos, and R. Shetter (2001), Chemical characterisation of pollution layers over the tropical Indian Ocean: Signatures of biomass burning emissions, *J. Geophys. Res.*, *106(D22)*, 28,497–28,510.

Streets, D., et al. (2003), An inventory of gaseous and primary aerosol emissions in Asia, *J. Geophys. Res.*, *108*(D21), 8809, doi:10.1029/2002JD003093.

Tiedtke, M. (1989), A comprehensive mass flux scheme for cumulus parameterization in large-scale models, *Q. J. R. Meteor. Soc.*, *107*, 1779–1800.

van Leer, B. (1977), Towards the ultimate conservative difference scheme: IV. A new approach to numerical convection, *J. Comput. Phys.*, *23*, 276–299.

Wagner, F., D. Müller, and A. Ansmann (2001), Comparison of the radiative impact of aerosols derived from vertically resolved (lidar) and vertically integrated (sunphotometer) measurements: Example of an Indian aerosol plume, *J. Geophys. Res.*, *106(D19)*, 22,861–22,870.

O. Boucher, and B. Crouzille, Laboratoire d'Optique Atmosphérique,CNRS/ Université des Sciences et Technologies de Lille, 59655 Villeneuve d'Ascq, Cedex, France (boucher@loa.univ-lille1.fr; crouzill@loa.univ-lille1.fr)

D. Müller, Institute for Tropospheric Research, Permoserstr. 15 04318 Leipzig, Germany (detlef@tropos.de)

P. Chazette, Laboratoire des Sciences du Climat et de l'Environnment, CEA/CNRS, Gif-sur-Yvette, 91191 Gif sur Yvette, Cedex, France (pch@lsce.saclay.cea.fr)

C. Venkataraman, and S. Verma, Department of Chemical Engineering, Indian Institute of Technology, Bombay, Mumbai-400 076, India (chandra@iitb.ac.in; shubha@iitb.ac.in)

M. S. Reddy, University Corporation for Air Research, NOAA-Geophysical Fluid Dynamics Laboratory, Princeton Forrestal Campus, 201 Forrestal Road, Princeton NJ, 08540 (shekar.reddy@noaa.gov)